Electronic Supplementary Material (ESI) for Nanoscale.
This journal is © The Royal Society of Chemistry 2018

Supplementary information

Self-passivated ultra-thin SnS layers via mechanical exfoliation and post-oxidation

Naoki Higashitarumizu[1], Hayami Kawamoto[1], Masaru Nakamura[2], Kiyoshi Shimamura[2], Naoki Ohashi[2], Keiji Ueno[3] and Kosuke Nagashio[1*]

[1]Department of Materials Engineering, The University of Tokyo, Tokyo 113-8656, Japan

[2]National Institute for Materials Science (NIMS), Tsukuba, Ibaraki 305-0044, Japan

[3]Department of Chemistry, Saitama University, Saitama 338-8570, Japan

[*]E-mail: nagashio@material.t.u-tokyo.ac.jp

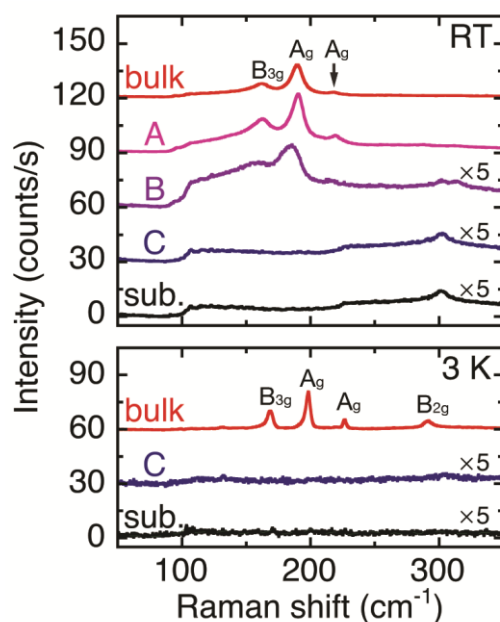

Fig. S1 Raman spectra measured at the points A, B, and C in Fig. 1b. The Raman spectrum of the SiO_2/Si substrate is also shown.

In the Raman spectra of the bulk flake (~432 nm thick) at RT, as shown in **Fig. S1**, specific peaks of SnS were observed at 161.7, 189.6 and 218.3 cm^{-1}, which are consistent with the reported values.[1–3] With a reduction in the thickness from bulk to A to B, the sharp spectrum became broader with a redshift. The broadening and redshift are considered to be due to a phonon confinement owing to the thinning effect.[4,5] When the flake thickness further decreased to 4.3 nm (point C), Raman spectrum suddenly disappeared at RT and was not recovered even at 3 K. In contrast, a clear spectrum was observed for the bulk SnS with a smaller full-width at half-maximum and larger intensity at 3 K, compared with that at RT. These results indicate that the disappearance of Raman peaks below a critical thickness of 4.3 nm originates from the surface modification rather than the detection limit of Raman measurement.

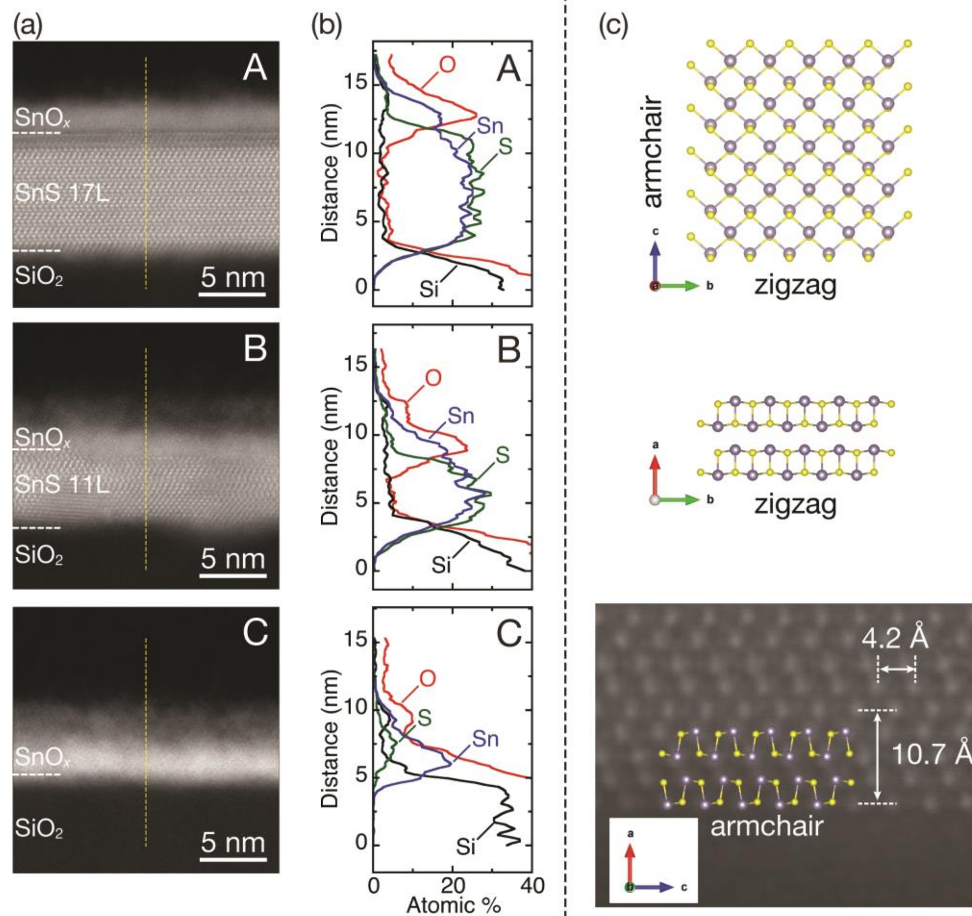

Fig. S2 (a) Cross-sectional HAADF-STEM images of SnS flakes at the points A, B, and C in **Fig. 1b**. (b) EDS depth profiles of SnS flakes along the dashed lines in Fig. S2a. (c) Crystal structure of SnS from *a*, *b*, and *c* axis. Enlarged cross-sectional HAADF-STEM image at the point A is also shown in comparison with a crystal structure model along the armchair direction. Sn and S atoms are shown in grey and yellow, respectively.

The a-SnO_x/SnS hetero-structure was also observed for the point B (10.5 nm), as well as point A (13.8 nm), whereas only the a-SnO_x layer was observed for the point C (4.3 nm), lacking apparent crystallinity. Notably, the HAADF-STEM image of the point B is more ambiguous than that of the point A, because it was difficult to obtain a clear electron diffraction image with the decrease in the flake thickness owing to the in-plane fluctuation, which originates from the surface roughness of the SiO_2/Si substrate. As shown in **Fig. S2c**, the atomic configurations of SnS layers correspond to those of 2D SnS grown via physical vapor deposition and bulk SnS along the armchair *c* axis direction,[2,3,6–10] where the largest carrier mobility can be obtained.[11,12] The lattice constants were determined to be a = 10.7 Å and c = 4.2 Å, consistent with the reported values.[8–10] The numbers of SnS layers at the points A and B were determined to be 17 and 11 (17L and 11L), respectively.

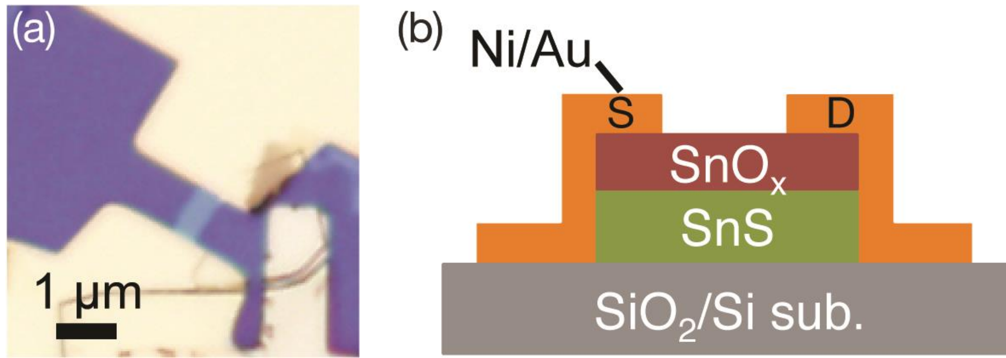

Fig. S3 (a) Typical optical image and (b) cross-sectional illustration of back-gated SnO_x/SnS FET.

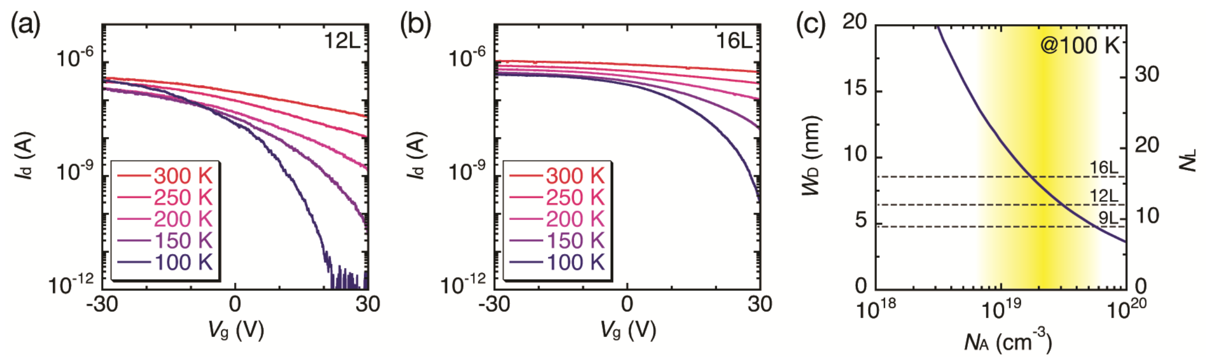

Fig. S4 I_d–V_g plots of (a) 12L and (b) 16L SnS FETs in the temperature range 300–100 K. (c) Relationship between depletion width W_D and acceptor density N_A at 100 K. N_L is the number of SnS layers, which corresponds to W_D. The highlighted region shows the estimated N_A of SnS.

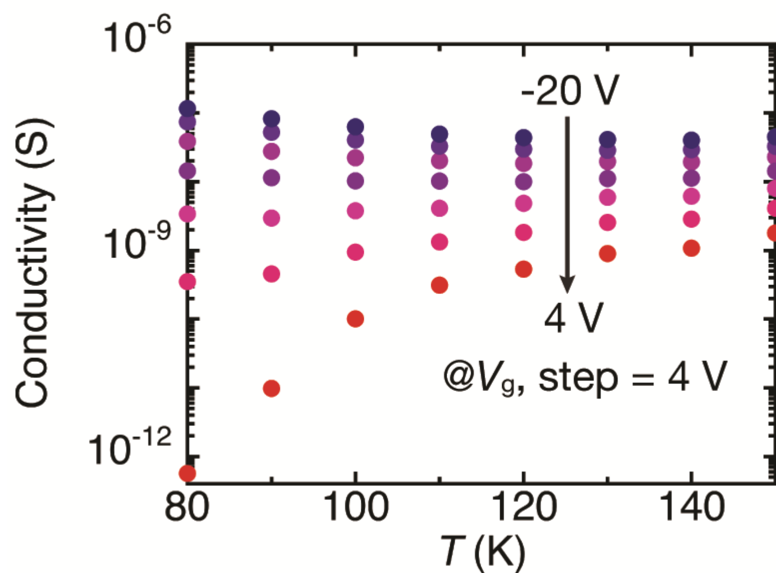

Fig. S5 Two-probe conductivity as a function of temperature for the 9L SnS fabricated via Au-exfoliation.

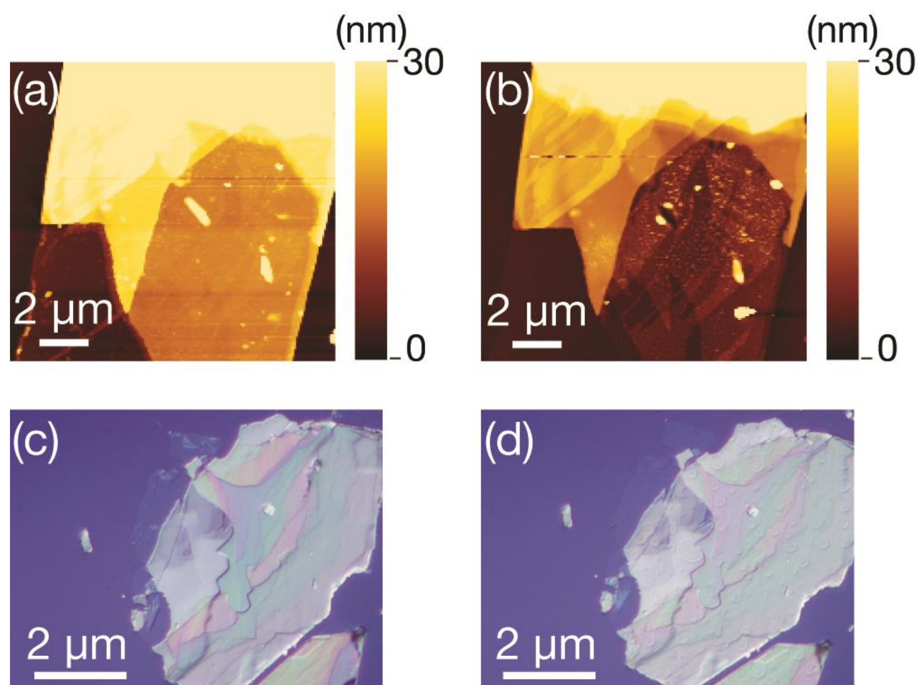

Fig. S6 (a,b) AFM topographic images of SnS flakes (a) before and (b) after O_2 plasma treatment at RT with the radio frequency power of 300 W for 450 sec. (c,d) Optical images with Normarski interference contrast of SnS flakes (c) before and (d) after ozone treatment at 200°C for 1 h.

Table 1 Typical etching rates of SnS in the early stage of annealing (<20 min) at different temperatures.

Temperature (°C)	350	380	410	430
Etching rate (nm/min)	<0.1	0.9	2.0	>10

References

1 H. R. Chandrasekhar, R. G. Humphreys, U. Zwick and M. Cardona, *Phys. Rev. B*, 1977, **15**, 2177–2183.

2 J. Xia, X.-Z. Li, X. Huang, N. Mao, D.-D. Zhu, L. Wang, H. Xu and X.-M. Meng, *Nanoscale*, 2016, **8**, 2063–2070.

3 M. Li, Y. Wu, T. Li, Y. Chen, H. Ding, Y. Lin, N. Pan and X. Wang, *RSC Adv.*, 2017, **7**, 48759–48765.

4 Y. Kanemitsu, H. Uto, Y. Masumoto, T. Matsumoto, T. Futagi and H. Mimura, *Phys. Rev. B*, 1993, **48**, 2827–2830.

5 Y. Sun, Z. Sun, S. Gao, H. Cheng, Q. Liu, F. Lei, S. Wei and Y. Xie, *Adv. Energy Mater.*, 2014, **4**, 1300611.

6 S. Sucharitakul, U. Rajesh Kumar, R. Sankar, F.-C. Chou, Y.-T. Chen, C. Wang, C. He, R. He and X. P. A. Gao, *Nanoscale*, 2016, **8**, 19050–19057.

7 Z. Tian, C. Guo, M. Zhao, R. Li and J. Xue, *ACS Nano*, 2017, **11**, 2219–2226.

8 M. Nakamura, H. Nakamura, M. Imura, S. Otani, K. Shimamura and N. Ohashi, *J. Alloys Compd.*, 2014, **591**, 326–328.

9 D. R. Lide, *CRC Handbook of Chemistry and Physics, Internet Version*, CRC press, Boca Raton, 2005.

10 S. Del Bucchia, J. C. Jumas and M. Maurin, *Acta Crystallogr. Sect. B*, 1981, **37**, 1903–1905.

11 C. Xin, J. Zheng, Y. Su, S. Li, B. Zhang, Y. Feng and F. Pan, *J. Phys. Chem. C*, 2016, **120**, 22663–22669.

12 L.-C. Zhang, G. Qin, W.-Z. Fang, H.-J. Cui, Q.-R. Zheng, Q.-B. Yan and G. Su, *Sci. Rep.*, 2016, **6**, 19830.